Significance of the balance between intracellular glutathione and polyethylene glycol for successful release of small interfering RNA from gold nanoparticles

Citation: McCully, Mark, Yulan Hernandez, João Conde, Pedro V. Baptista, Jesus M. de la Fuente, Andrew Hursthouse, David Stirling, and Catherine C. Berry. "Significance of the Balance Between Intracellular Glutathione and Polyethylene Glycol for Successful Release of Small Interfering RNA from Gold Nanoparticles." Nano Research 8, no. 10 (August 28, 2015): 3281–3292.

As Published: http://dx.doi.org/10.1007/s12274-015-0828-5

Publisher: Tsinghua University Press

Persistent URL: http://hdl.handle.net/1721.1/105547

Version: Author's final manuscript: final author's manuscript post peer review, without publisher's formatting or copy editing

Nano Research 2015, 8(10): 3281–3292
DOI 10.1007/s12274-015-0828-5
Research Article
ISSN 1998-0124
CN 11-5974/O4

Significance of the balance between intracellular glutathione and polyethylene glycol for successful release of small interfering RNA from gold nanoparticles

Mark McCully[1] (✉), Yulan Hernandez[2], João Conde[3], Pedro V. Baptista[4], Jesus M. de la Fuente[2,5,6], Andrew Hursthouse[7], David Stirling[7], and Catherine C. Berry[1]

[1] *Centre for Cell Engineering, University of Glasgow, Glasgow, G12 8QQ, Scotland, UK*
[2] *Institute of Nanoscience of Aragon, University of Zaragoza, Zaragoza 50018, Spain*
[3] *Massachusetts Institute of Technology, Institute for Medical Engineering and Science, Harvard-MIT Division for Health Sciences and Technology, Cambridge, Massachusetts 02139, USA*
[4] *UCIBIO, Departamento de Ciências da Vida, Faculdade de Ciências e Tecnologia, Universidade Nova de Lisboa, Campus de Caparica, Caparica 2829-516, Portugal*
[5] *Instituto de Ciencia de Materiales de Aragón (ICMA), CSIC-Universidad de Zaragoza, c/Pedro Cerbuna 12, Zaragoza 50009, Spain*
[6] *Institute of Nano Biomedicine and Engineering, Key Laboratory for Thin Film and Microfabrication Technology of the Ministry of Education, Research Institute of Translation Medicine, Shanghai Jiao Tong University, Dongchuan Road 800, Shanghai 200240, China*
[7] *School of Science, University of the West of Scotland, Paisley, PA1 2BE, Scotland, UK*

Received: 12 February 2015
Revised: 3 June 2015
Accepted: 5 June 2015

KEYWORDS
gold,
nanoparticles,
PEG,
glutathione,
siRNA,
drug delivery

ABSTRACT

The therapeutic promise of small interfering RNAs (siRNAs) for specific gene silencing is dependent on the successful delivery of functional siRNAs to the cytoplasm. Their conjugation to an established delivery platform, such as gold nanoparticles, offers tremendous potential for treating diseases and advancing our understanding of cellular processes. Their success or failure is dependent on both the uptake of the nanoparticles into the cells and subsequent intracellular release of the functional siRNA. In this study, utilizing gold nanoparticle siRNA-mediated delivery against C-MYC, we aimed to determine if we could achieve knockdown in a cancer cell line with low levels of intracellular glutathione, and determine the influence, if any, of polyethylene glycol (PEG) ligand density on knockdown, with a view to determining the optimal nanoparticle design to achieve C-MYC knockdown. We demonstrate that, regardless of the PEG density, knockdown in cells with relatively low glutathione levels can be achieved, as well as the possible effect of steric hindrance of PEG on the availability of the siRNA for cleavage in the intracellular environment. Gold nanoparticle uptake was demonstrated via transmission electron microscopy and mass spectroscopy, while knockdown was determined at the protein and physiological levels (cells in S-phase) by in-cell westerns and BrdU incorporation, respectively.

Address correspondence to Mark.McCully4@gmail.com

1 Introduction

With recent advances in gene discovery and analysis, the relationship between gene dysfunction and disease phenotype is being unraveled. Gene therapy has therefore become an attractive area of research, by targeting diseases at the genetic level. Small interfering RNAs (siRNAs) are double-stranded RNAs approximately 20–25 nucleotides long that are involved in the RNA interference pathway. siRNAs bind specifically, with complete complementarity, to their target RNA sequences, halting their expression; thus, they offer an attractive mechanism for successful and specific gene therapy [1]. A report by Derfus et al. indicated that one siRNA molecule per particle conjugated with >15 peptides produced optimal knockdown and targeting [2].

However, the clinical translation of gene therapy has been set back due to technical issues surrounding the delivery of genetic material. When considering siRNA delivery, the main steps towards successful delivery include: (1) cellular localization and binding, (2) cellular internalization, (3) subcellular trafficking and endosomal escape, and (4) release of functional siRNA capable of interaction with the RISC complex (containing cellular machinery for silencing to progress) [3]. Therefore, there is a pressing need to design a delivery platform capable of protecting siRNA from degradation and safely delivering it to target cells while maintaining its functionality.

To this end, nanoparticles have been hailed as a revolutionary vehicle for targeted cellular delivery. Gold nanoparticles (AuNPs) in particular have become popular in biomedicine; aside from their unique physical and chemical properties, they are biologically inert and have a history of biomedical use that spans decades [4]. AuNPs have the additional advantage of being easily synthesized, with excellent control over size, shape, stability, and surface modification [4]. The choice of ligands on the nanoparticle surface and their molecular size and organization will influence their biological properties, and careful design is required.

Polyethylene glycol (PEG) is often utilized to passivate AuNPs for biological use, owing to its inherent protein repulsion tendency. The steric tethering of PEG chains to AuNPs confers ideal stability under physiological conditions, while minimizing interaction with biomacromolecules, which might otherwise lead to aggregation. This protein repulsion tendency of PEG does not depend on the nature of PEG binding to the NP, as both covalently and electrostatically bound PEG show good protein rejection capacity; however, stronger binding can ensure that PEG functionality is not lost [5]. To date, when utilizing PEG, researchers have focused on the importance of the PEG chain length, as it has been established that shorter chains provide enhanced cellular uptake [6]. There are mixed reports with respect to PEG chain density on the surface of an NP, mainly due to both the branching effect and overall molecular weight. Hypothetically, a higher molecular weight may provide better flexibility (through long chain molecules), but this will also make the NP larger and restrict attachment of additional ligands. It is therefore generally thought that a high density of short-chain PEGs is preferred for achieving optimum cellular uptake while maintaining the PEGylated particle's stealth properties [5].

A final, and critical, consideration in the AuNP design is the intracellular release of functional siRNA from the AuNP surface. Here, the strong thiol-Au interaction is readily exploited to allow exchange between –S/Au- and thiol-containing molecules such as glutathione in the cytoplasm, leading to efficient dissociation from the gold surface [7]. Glutathione (GSH) is an abundant thiol-containing compound in most cells, and is found in the millimolar range in the cytoplasm of healthy cells, making it an excellent candidate for GSH-triggered siRNA release [8].

Functionalized AuNPs are therefore highly promising vehicles for gene therapy, as they can be synthesized with a view to protecting the genetic material from degradation and demonstrate efficient uptake, while also being designed to target specific cell types [9–11]. In previous work, we have demonstrated that AuNPs with a low concentration of PEG functionalized with thiolated siRNA were capable of inducing C-MYC knockdown in HeLa cells [12]. In the present study, with regards to AuNP functionality, our aims were twofold: (i) to determine if we could achieve C-MYC knockdown in a cancerous cell line that contains a lower intracellular GSH concentration than HeLa cells,

and (ii) to determine the importance of the degree of saturation of the PEG layer in terms of siRNA release within the cells. To this end, the bone carcinoma cell line MG63 [12] was employed in this study, and challenged with AuNPs with two PEG densities: 25% and 40%. The results demonstrate that, while MG63s exhibited relatively lower GSH levels compared to other cancer cell lines, C-MYC knockdown was still achieved. Interestingly, a variation in efficacy was noted that favored the lower 25% PEG density. At the higher concentration of 15 nM, the 25% PEG-containing AuNPs induced a significantly better knockdown in C-MYC protein, with similar trends in cell proliferation levels. Conversely, at the lower concentration of 2 nM, while protein knockdown was comparable, a significantly greater reduction in cell proliferation was noted with 25% PEG. Following the comparison of intracellular GSH levels in MG63 cells, and two other established cancer cell lines (MCF-7 and HeLa), it was surmised that perhaps the considerably lower GSH levels found in MG63 cells render the cells less able to access the siRNA at the higher PEG density of 40%. This observation suggests that the required GSH-thiol interaction that is needed for siRNA release within the cell is finely balanced, and must be addressed when designing NPs for therapeutic use.

2 Materials and methods

2.1 Synthesis and functionalization of gold nanoparticles

AuNPs with a diameter of 14 nm were synthesized by the citrate reduction method described by Turkevich and Frens in Refs. [13–15]. A mixture of AuNPs, 0.028% SDS, and HS-EG(8)-$(CH_2)_2$-COOH (Iris-Biotech) (M_W = 458 Da) and HS-$(CH_2)_3$-CONH-EG(6)-$(CH_2)_2$-N3 (synthesized in our lab) (M_W = 452 Da) in a 1:1 ratio (7 and 10.5 μM of each chain for 25% and 40%, respectively) was combined under basic conditions for 16 h. PEGylated AuNPs (~8 PEG unit lengths) were obtained after purification by centrifugation. Quantification of the number of PEG molecules attached was performed by Ellman's method by calculating the excess thiolated PEG chains found in the supernatant. For fine tuning the PEG density, different amounts of PEG-COOH were used in the experiment (the presence of PEG-N3 had already been demonstrated by our group in Ref. [12]). The AuNPs obtained were characterized by UV-Vis spectroscopy, transmission electron microscopy (TEM), zeta potential, and dynamic light scattering (DLS).

Further chemical functionalization with biotin (labeled as B) was performed using 1-ethyl-3-(3-dimethylaminopropyl)carbodiimide (EDC) (Sigma-Aldrich) and sulfo-hydroxysuccinimide (sulfo-NHS) (Sigma-Aldrich) chemistry at pH 6.1 (25 mM MES). AuNP was functionalized with siRNA (Thermo Scientific Dharmacon) (labeled as S) using thiolated siRNA previously reduced with dithiothreitol (DTT) incubated with AuNPs followed by the addition of 0.028% SDS and NaCl at a final concentration of 0.1 M (25% saturated AuNPs) or 0.3 M (40% saturated AuNPs). Excess siRNA was removed by centrifugation at 4 °C. siRNA was quantified by fluorescence measurement of supernatants (Perkin-Elmer LS55) using GelRed (Biotium), a nucleic acid intercalator, after establishing a calibration curve with the thiolated siRNA used (Emission at 602 nm = 7,328.3 × [siRNA, n mol] + 39.366). The panel of four AuNPs and PEG chain densities employed in this study are described in the legend (with associated acronyms) in Table 1, with a schematic illustrating the ligands attached to the 25% and 40% PEG saturated AuNPs shown in Fig. 1.

Table 1 A complete list of the AuNPs used in this study and the corresponding PEG ligand densities. Please note that B denotes biotin and S denotes siRNA

	Nanoparticle type	PEG ligand density (chains per nm^2)
1	Au-B-25% PEG	~ 2.03
2	Au-B-S-25% PEG	~ 2.03
3	Au-B-40% PEG	~ 2.99
4	Au-B-S-40% PEG	~ 2.99

2.2 Cell culture

The human osteosarcoma cell line MG63 was cultured in DMEM growth medium (10% fetal bovine serum, 2 mM glutamine, 100 U/mL penicillin, and 100 μg/mL streptomycin) and maintained at 37 °C in 5% CO_2 until ~90% confluent, after which they were passaged

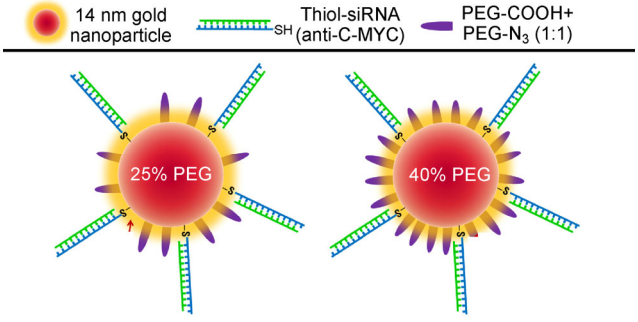

Figure 1 Schematic of the 25% and 40% PEG saturated AuNPs with associated ligands.

and counted with a hemocytometer. Cells were seeded at a density of 1 × 10^4 cells per mL for experiments unless stated otherwise. Cells were cultured for 24 h before the addition of both the 25% and 40% PEG AuNP treatments at 2 and 15 nM.

2.3 GSH assay

The MG63 cells employed in this study and two other established cancer cell lines, HeLa and MCF-7, were cultured and harvested (1 × 10^6 cells were collected for each cell line) to determine cytoplasmic GSH levels. The cells were lysed with lysis buffer (GSH kit obtained from AbCam), incubated on ice for 10 min, and centrifuged at 13,000*g* for 10 min. A standard GSH curve was prepared alongside the samples. Monochlorobimane [16], a dye that forms an adduct with GSH, was added to the well and the plate was incubated for 1 h at 37 ˚C. The fluorescence was measured using a plate reader with EX/EM = 360/420 nm.

2.4 Toxicity

Cytotoxicity was assessed by a standard MTT (3-(4,5-dimethylthiazol-2-yl)-2,5-diphenyltetrazolium bromide) assay. Cells were seeded in a 96-well plate in triplicate. Following incubation with the AuNPs, cells were incubated in 100 μL of MTT solution (Sigma- Aldrich; 5 mg/mL in phosphate-buffered saline (PBS)) for 60 min at 37 ˚C, after which the MTT was aspirated off and 100 μL of dimethyl sulfoxide (Thermo Fisher Scientific, Waltham, MA) was added for 10 minutes. The plate was subsequently read via spectrophotometry (Dynatech MR7000 at 550 nm).

2.5 Cellular uptake of AuNPs

2.5.1 Inductively coupled plasma mass spectrometry (ICP-MS)

Cells were seeded (100 μL/well) in a 96-well plate and incubated for 24 h, followed by the addition of AuNPs and an additional 48-h incubation. The media were transferred to 1 mL H_2O (Millipore Ultra-Pure), followed by the addition of 1 mL of 70% HNO_3 and incubation overnight in a 70 ˚C water bath. Samples were adjusted to 50 mL with Millipore Ultra-Pure water and analyzed by ICP-MS at the University of West Scotland (Paisley, UK). The converted values for gold uptake were averaged (n = 3) and used for statistical analysis.

2.5.2 TEM

Cells were seeded at a density of 4 × 10^4 cells per mL onto Thermanox coverslips (13 mm in diameter) and cultured to develop a confluent monolayer of cells. At this point, the AuNPs were added and cells were cultured for another 24 h. Cells were subsequently fixed with 1.5% glutaraldehyde in phosphate buffer (1.15 g/L Na_2HPO_4, 0.2 g/L KH_2PO_4, 8 g/L NaCl and 0.2 g/L KCl) for 2 h, and washed for 10 min with PBS. Cells were then post-stained for 60 min with 1% osmium tetroxide in phosphate buffer, post-fixed in 1% buffer followed by 0.5% uranyl acetate for 1 h, and then dehydrated in increasing concentrations of alcohol and left in resin (propylene oxide Epon 812 resin mix (1:1)) overnight. Cell layers were captured in pure resin and cured overnight in an oven. Blocks were then cut into ultrathin sections, stained with 2% methanolic uranyl acetate and Reynolds lead citrate, and viewed under a Leo 912 AB TEM (120 kV for cells).

2.6 C-MYC knockdown

2.6.1 In-cell western (ICW)

Cells were seeded in a 96-well plate in triplicate, challenged with the AuNPs for 24 and 48 h, then fixed, permeabilized, and blocked as in section 2.5. Samples were then co-incubated with primary antibodies (1:10,000 mouse anti-C-MYC, [9E10], ChIP Grade (ab32), AbCam and 1:10,000 rabbit anti-GAPDH, Epitomics)

at 37 ˚C for 1 h. Following washing with PBS/Tween, samples were co-incubated with secondary antibodies (1:10,000 donkey anti-mouse IR680RD, LI-COR Biosciences, Cambridge, UK and 1:10,000 donkey anti-rabbit IR800CW, LI-COR Biosciences) at 37 ˚C for 1 h. All samples were finally washed three times in PBS/Tween (5 min per wash). The plates were imaged by scanning simultaneously at 700 and 800 nm with an Odyssey SA at 100 μm resolution, medium quality, focus offset of 3.53 mm, and an intensity setting of 7 for both 700- and 800-nm channels.

2.6.2 *BrdU proliferation assay*

Cells were seeded onto 13-mm glass coverslips for 24 h, and further incubated with AuNPs for 42 h. After this time, 1 mM BrdU (Sigma-Aldrich) solution was added and the cells cultured an additional 6 h. The media were removed and cells were washed in PBS, fixed, permeabilized, and blocked as in section 2.5. Anti-BrdU antibody (Cell Proliferation Kit RPN20, GE Healthcare, Buckinghamshire, UK) was diluted 1:100 in DNase I and added and the cells were incubated for 2.5 h at 37 ˚C. Cells were then washed 3 times before incubating with Texas Red-conjugated anti-mouse antibody (1:50 in PBS/1% bovine serum albumin) for 1 h. Cells were finally mounted and stained with DAPI (Vector Laboratories). Cells were imaged using an Axiovert 200m fluorescence microscope (Carl Zeiss, Jena, Germany) equipped with ImagePro Plus Version 6.01 software (Media Cybernetics) and a sideport-mounted Evolution QEi Monochrome CCD camera (Media Cybernetics).

2.7 Statistics

Statistical analysis was performed in GraphPad using one-way ANOVA and Dunnett's post-test. In all figures * = $p < 0.05$, ** = $p < 0.01$, *** = $p < 0.001$, and **** = $p < 0.0001$. Two-tailed t-tests were performed where specifically mentioned using Welch's correction: = $p < 0.05$, = $p < 0.01$

3 Results

3.1 Synthesis and functionalization of AuNPs

AuNPs were synthesized using Turkevich and Fren's method and subsequently functionalized with different amounts of thiolated PEG chains in order to achieve different densities of the PEG layer surrounding the AuNP core. The quantification of the attached PEG chains was made by quantification of the free thiol groups present on the supernatants after purification by Ellman's assay. A complete study was performed using PEG-COOH to generate a corresponding saturation curve of the surface of the AuNP (Fig. 2(a)). The presence of the PEG-N3 had already been tested for different amounts of PEG in previous work by our group in Ref. [12]. These AuNPs (Au 25% PEG and Au 40% PEG) were further characterized by TEM, DLS, and zeta potential (Figs. 2(b1)–2(b3)).

The terminal carboxylic groups of PEG chains were subsequently functionalized with aminated biotin through a carbodiimide-induced coupling reaction. Finally, thiolated siRNA was directly bound to the AuNP core in the presence of SDS and subsequent additions of salt up to 0.1 M for Au-B 25% PEG and to 0.3 M for Au-B 40% PEG. While the same amounts of thiolated siRNA were used for both the 25% and 40% PEG AuNPs, it should be noted that a slightly higher level of siRNA ligands might attach to the 25% sample (due to the different salt concentrations used in synthesis). The amount of thiolated siRNA attached was calculated by measuring the excess siRNA in the supernatants after adding GelRed. The stability of all samples was monitored at each step by UV–Vis spectroscopy (Fig. 2(c)).

3.2 Intracellular GSH levels

The NPs were designed based on the established AuNP/GSH interaction within the cytoplasm, whereby GSH cleaves thiol bonds that in turn release the thiolated siRNA from the gold core. The levels of GSH in the current cell line, MG63, were determined and compared to GSH levels in both HeLa and MCF-7 cancer cell lines (Fig. 3 and Table S1 in the Electronic Supplementary Material (ESM)). MG63 cells were found to have relatively low GSH levels in comparison to both MCF-7 and HeLa cells, with that of HeLa cells being approximately 4 times higher (Fig. 3). From previous studies, we established that C-MYC knock-down in HeLa cells using thiol exchange via GSH was easily achievable; therefore, MG63 were selected

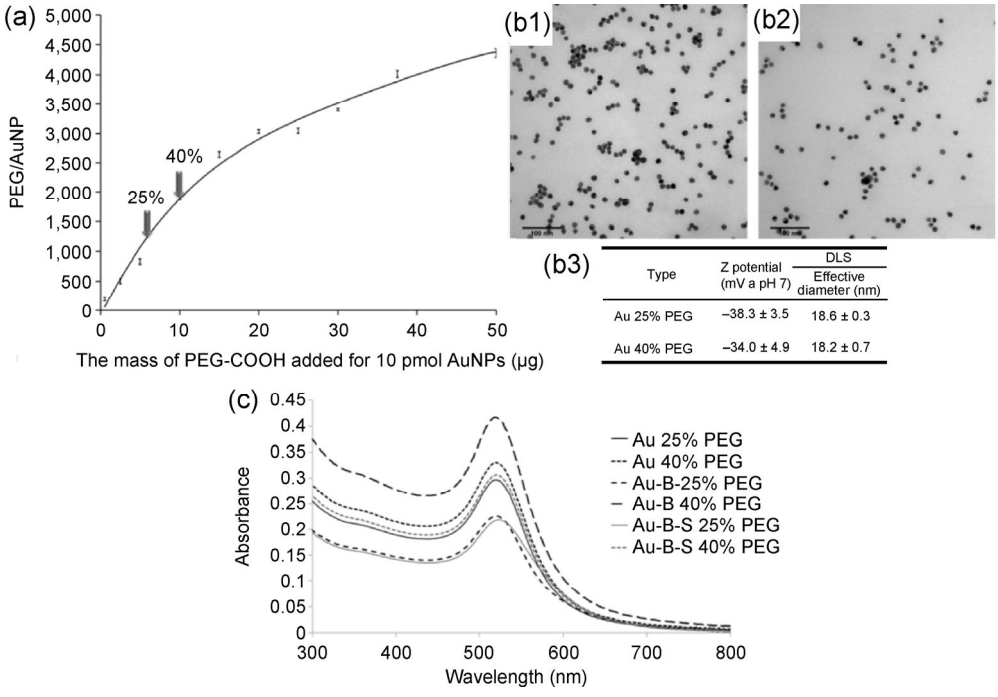

Figure 2 Study of the saturation of the AuNP's surface with PEG chains (a), characterization of the 25% PEG saturated (b1) and 40% PEG saturated (b2) AuNPs by TEM, and by zeta potential and DLS (b3); UV–Vis spectrum of all the AuNPs used in this study (c).

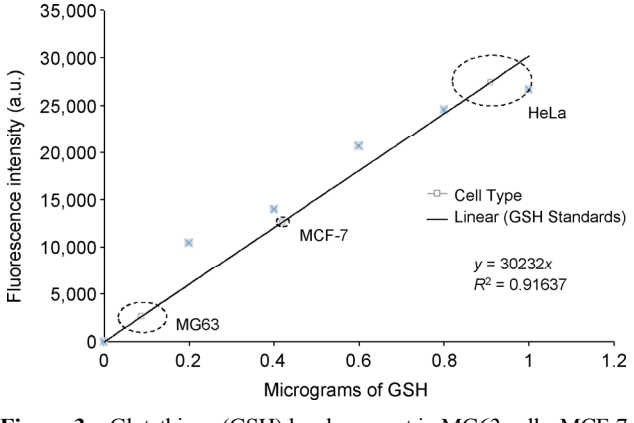

Figure 3 Glutathione (GSH) levels present in MG63 cells, MCF-7, and HeLa cancer cell lines. Cell number was normalized to 1×10^6 cells and values were plotted onto a GSH standard curve ($n = 3$). Crosses indicate GSH standards, while the squares correspond to the cell type. Dashed areas around cell type indicate SD.

to test the level of functionality achievable with our siRNA-AuNPs in a cancer cell line of known lower GSH concentration.

3.3 Toxicity: MTT assay

The AuNPs were found to have no cytotoxicity over 24 h of incubation, as demonstrated by the MTT assay, showing no statistical difference between treatments (Fig. 4).

3.4 Cellular uptake of AuNPs

To examine AuNP uptake in greater detail, TEM with cross-sectional imaging was used. At the lower 25% PEG saturation, the AuNPs were all distinctly located in the cytoplasm, and perhaps more apparent at the higher 15 nM concentration (Fig. 5). Images for the 40% PEG saturation were similar, again with AuNPs evident in the cell body (Fig. 6). The NPs were evident within the cell after 24 h of incubation.

In parallel with qualifying AuNP uptake into cells, the amount of AuNPs within the cells was also quantified after 24 h using ICP-MS to determine elemental gold levels in lysed cell samples. All AuNP types were recorded in the cells (Fig. 7). Clear evidence was shown that more AuNPs were present at the higher concentration, confirming the validity of the method. Between the AuNP species at both concentrations, there was no significant difference between the 25% and 40% PEG with regards to uptake (unpaired t-test with Welch's correction).

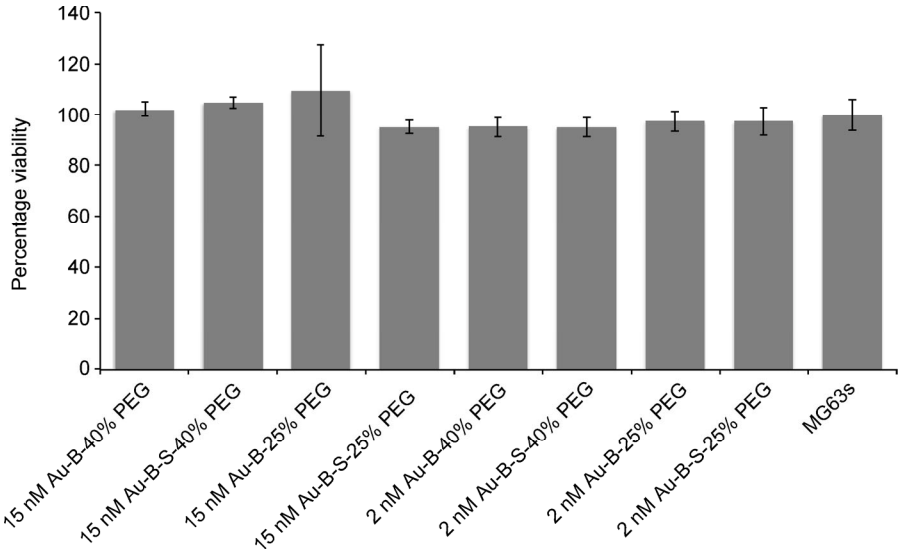

Figure 4 MTT analysis of MG63 cells treated with 15 and 2 nM of each AuNP, with 40% or 25% PEG coverage for 24 h (B = biotin; S = siRNA). Samples were normalized to MG63s without AuNPs (n = 3; error bars indicate SD).

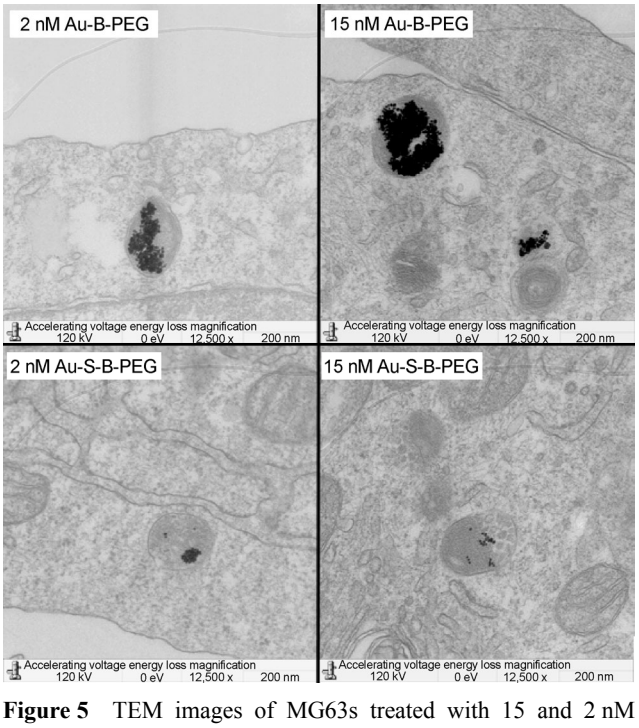

Figure 5 TEM images of MG63s treated with 15 and 2 nM AuNPs, with 25% PEG after a 24-h incubation. Clusters of the AuNPs are evident within the cell body. Scale bar = 1 μm.

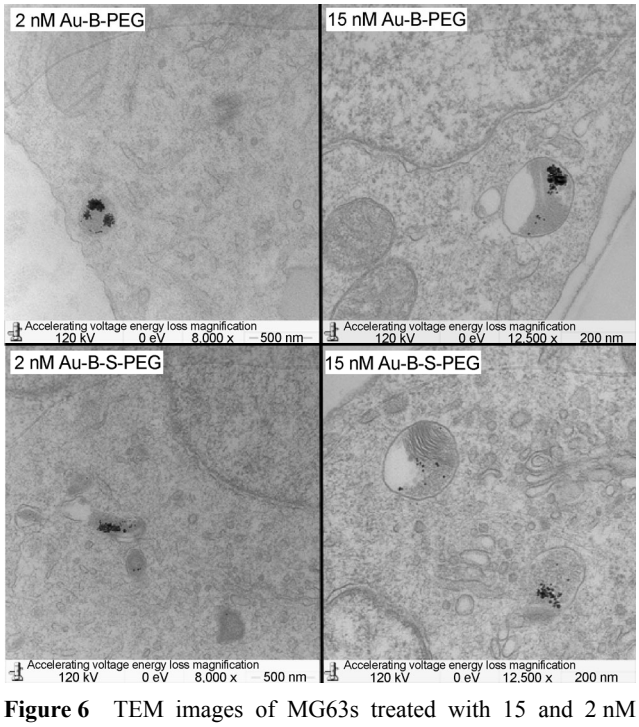

Figure 6 TEM images of MG63s treated with 15 and 2 nM AuNPs, with 40% PEG after a 24-h incubation. As with the 25% PEG-containing AuNPs, clusters of AuNPs are evident within the cell body.

3.5 siRNA-mediated C-MYC knockdown

Following verification and quantification of AuNP uptake into MG63 cells, the efficiency of siRNA-mediated C-MYC silencing was evaluated using ICW. The higher concentration (15 nM) produced knockdown at both PEG densities (25% and 40%); however, the 25% density was significantly more effective. The lower concentration (2 nM) produced comparable knockdown, with no difference noted between the densities. The optimal knockdown was achieved with

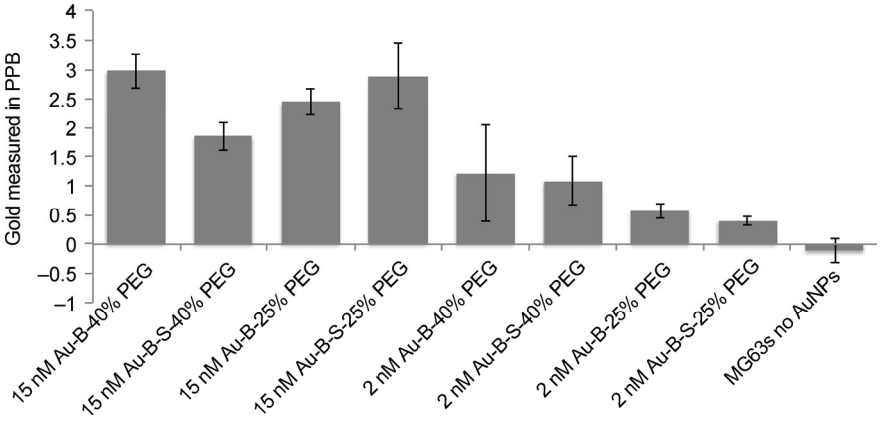

Figure 7 ICP-MS analysis of MG63s treated with 2 and 15 nM of AuNPs, with 25% or 40% PEG coverage for 24 h (n = 3 for each lysate, error bars denote SD). The higher concentration (15 nM) clearly led to higher gold levels in cells. All values have been normalized to that of ultrapure water.

a combination of both approaches, using the higher concentration (15 nM) and lower PEG density (25%) (Fig. 8). There was also a significant reduction in C-MYC protein noted for one of the controls, Allstar nonsense siRNA with Lipofectamine; however, this result may be due to the Lipofectamine affecting cell proliferation.

The synthetic nucleoside BrdU was used to analyze cells entering S-phase in the cell cycle, thus giving an indication of cell division in the sample population. As shown in Fig. 9, there was a higher proportion of cells in S-phase (red) in the standard control cells (with no AuNPs) and cells treated with the additional control NPs (biotin and PEG only), in contrast to the lack of any cell division detected in cells treated with the siRNA AuNPs (Fig. 9). To quantify this property, ten random images were obtained from each cell sample (n = 3 per sample) and the proportion of cells in S-phase was determined using Cell Profiler (Fig. 10). The results demonstrate a significant decrease in cells entering S-phase when treated with siRNA at the

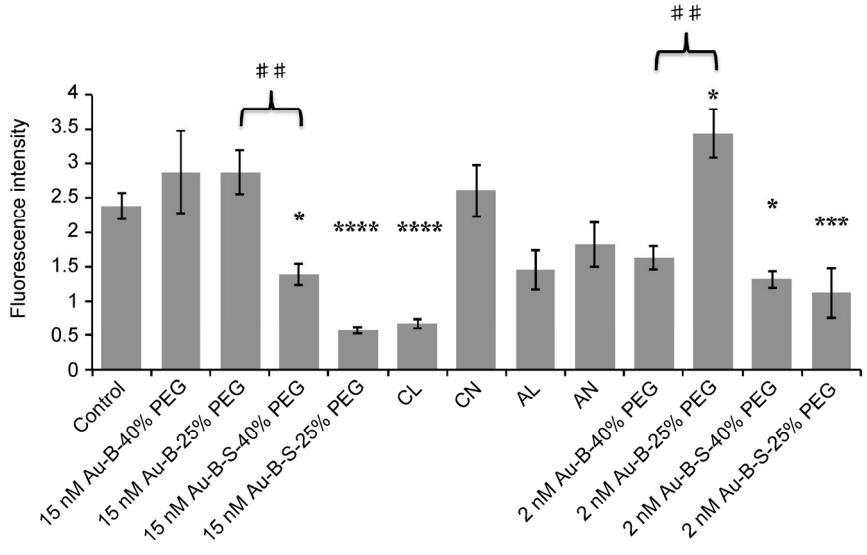

Figure 8 ICW data comparing C-MYC protein levels in MG63s with AuNP treatments, normalized to that of GAPDH. Cells were serum starved for 24 h before treatment to synchronize cell division. NPs were added at both 2 and 15 nM, with both 25% and 40% PEG coverage. The standard control reflects cells without AuNPs added. Additional controls included Lipofectamine alone, C-MYC siRNA with Lipofectamine (CL), Allstar nonsense siRNA with Lipofectamine (AL), or C-MYC siRNA or Allstar siRNA added directly to the media (CN & AN) (n = 6; error bars denote standard error, asterisk denotes significance based on ANOVA, with Dunnett's post-test for normalizing to controls. Hash marks indicate an unpaired two-tailed t-test with Welch's correction $p < 0.005$).

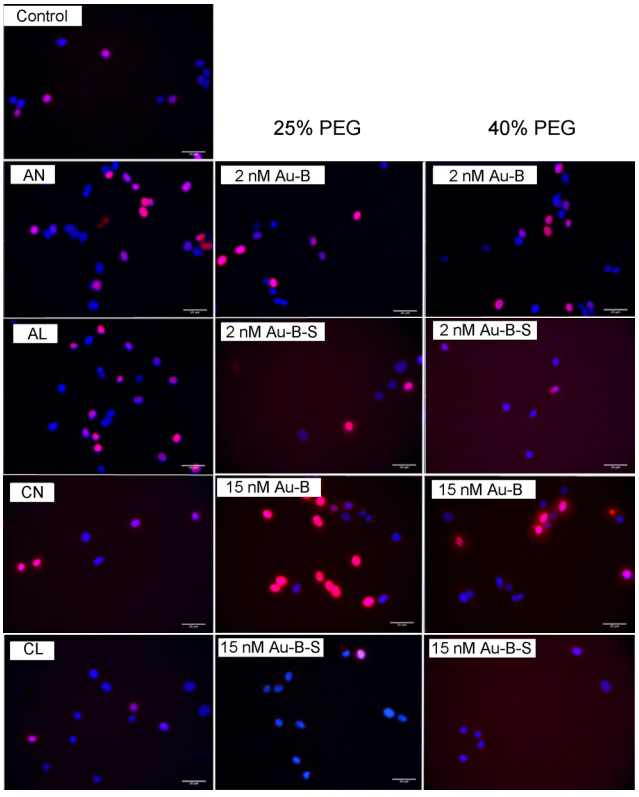

Figure 9 BrdU incorporation into cells treated with 2 and 15 nM AuNPs, with either 25% or 40% PEG coverage for 48 h. Cells were stained for nuclei (DAPI: blue) and actively dividing cells (BrdU: red). Additional controls included Lipofectamine alone, CL, AL, or CN & AN. Scale bar = 20 μm.

higher concentration (15 nM) at both PEG densities (25% and 40%), but cell proliferation was only decreased at the lower PEG density (25%) when tested at 2 nM.

4 Discussion

The use of intracellular GSH as a release mechanism has been capitalized upon with a view towards thiotethered ligand release from the surface of NPs [17–24]. While there have been several recent studies on the influence of the PEG chain length and ligand release [6], mixed reports on the effect of PEG density prompted this study, with a shorter chain length and higher density having been considered optimum for both ligand release and maintenance of the PEGylated particles' stealth properties [5].

Previous work involving our group has shown that PEGylated AuNPs functionalized with siRNA against C-MYC can knock down its expression in HeLa cells (2 nM with a PEG ligand density of 25%) [12]. The present study was designed to assess both the potency of the AuNPs, by assessing the knockdown in a cancer cell line with a lower intracellular GSH level, and the influence of PEG chain density on C-MYC knockdown. The NPs were PEGylated at both 25% and 40%, and were used at two concentrations, 2 and 15 nM. Following cellular toxicity and AuNP uptake assessment, C-MYC knockdown was determined.

When investigating C-MYC knockdown at the protein level, the higher concentration (15 nM) achieved clear knockdown at both 25% and 40% PEG density, with the lower 25% density achieving a significantly more pronounced knockdown (left-side values on the graph

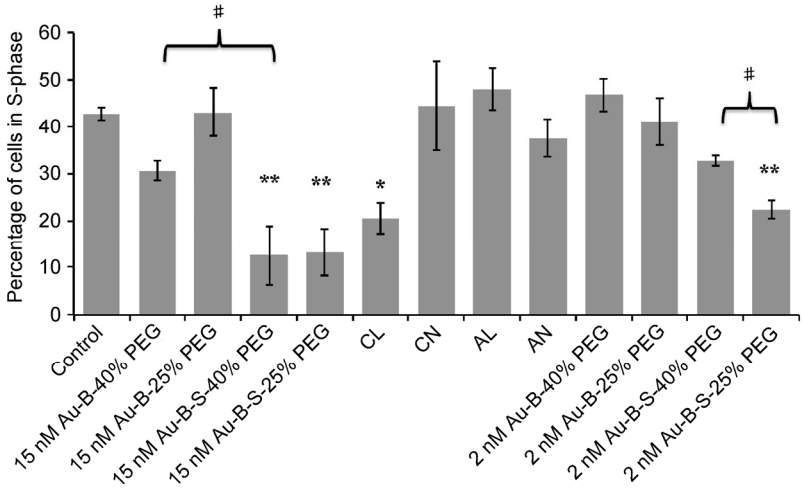

Figure 10 Graphical representation of the BrdU images as determined by Cell Profiler, normalized to nuclei number, comparing the level of MG63 cells in S-phase with different treatments (results from 10 images, $n = 3$ replicates, error bars denote standard error, asterisk denotes significance based on ANOVA with Dunnett's post-test to normalize to controls. Hash marks indicate unpaired two-tailed t-test with Welch's correction $p < 0.05$).

in Fig. 8). Meanwhile, the lower concentration (2 nM) also achieved knockdown at both densities, but to a lesser extent. At the physiological level, when determining changes in cell proliferation, the previously observed difference in protein knockdown evident at 15 nM was not apparent, with a comparable reduction in proliferation noted for both densities. However, for the lower concentration (2 nM), which produced a comparable protein knockdown, only the 25% PEG density resulted in a reduction in proliferation. Therefore, while the 25% PEG AuNPs have slightly higher levels of siRNA ligand attached, which may amplify this effect, these results still indicate that a variation in knockdown may be observed when adopting different PEG saturation densities, which may have consequences with regards to the therapeutic potential of siRNA.

GSH is an abundant thiol-cleaving enzyme located within cells. During normal cellular processes GSH exists in two distinct forms: oxidized (GSSH) and reduced (GSH). The oxidized form is <2% of total GSH levels [25]. GSH is used in many processes within the cells such as detoxification, removal of hydroperoxides, and maintaining oxidation of protein sulfhydryls [26–28]. Healthy cells tend to have GSH levels within the 1–10 mM range, an order of magnitude higher than in the extracellular environment [29]. Our AuNPs were designed with a view towards exploiting GSH's ability to cleave the thiol-conjugated siRNA. Increasing PEG length and ligand density to saturation can complicate access to the thiol [6], with greater ligand density or higher molecular weight polymers preventing access to the core [30]. Once released, the double-stranded siRNA is loaded into the RISC complex. Within the RISC complex, Ago2 cleaves the sense strand and dissociates it from the complex, after which it will ultimately be degraded [31]. The antisense strand, which is complementary to the target mRNA, will remain bound to the RISC complex until it recognizes the target sequence. Ago2 mediates the cleavage of the target mRNA ~10–11 nucleotides upstream of the guide strand's 5′ end. After degradation, the components of the RISC complex are recycled [32].

While ligand-based NPs are championed as holding great potential in future cancer diagnosis and therapy, they have thus far delivered inconsistent results. One of the major factors contributing to this inconsistency, along with other ligand issues, is thought to be differences in passivating PEG coatings on the NPs [6]. As discussed in the introduction, the PEG chain length is known to influence the NP-cell interactions; however, it is also well established that the PEG density on an NP surface can also affect the protein repelling capacity of the resultant NPs, and therefore influence the particles' stealth properties [33, 34]. The PEG density has also been identified as being key in determining cell uptake [6]. In the present study, the AuNPs with 40% PEG coverage demonstrated marginally lower uptake levels compared to the 25% PEG AuNPs (as demonstrated by ICP-MS results), and the TEM images indicated clear availability of the 40% PEG AuNPs in the cytoplasm. Thus, the 40% PEG density did not appear to hinder cellular uptake.

It is well established that ligand surface coverage, density, and conformation of functionalized NPs is of critical importance to the success of NP delivery systems; however, studies on these parameters have been lacking. Until only very recently, data on ligand densities on AuNPs (in the 10–100 nm range) were seldom reported [35]. This apparent paucity of data may be due in part to technical difficulties in obtaining such data, with X-ray crystallography and density functional theory studies being performed to derive theoretical considerations [36]. In this study, we surmise that the lower coverage of PEG potentially allowed greater access of the siRNA to the intracellular environment and the RISC complex, which was reflected in (i) the significantly reduced C-MYC protein levels recorded with 25% PEG at 15 nM (Fig. 8), and (ii) the reduction in cell proliferation observed with 25% PEG at 2 nM, while 40% PEG was similar to control levels (Fig. 10). The most pronounced C-MYC knockdown occurred using 15 nM and 25% PEG in tandem, which resulted in more efficient knockdown than that observed with positive control C-MYC Lipofectamine.

5 Conclusions

For siRNA to realize its therapeutic potential, it must be functional and freely available within the cytoplasm

to interact with the RISC complex. When relying on a GSH-based release strategy, this study highlights the importance of particle design, in terms of supporting ligand densities such as PEG, and intracellular GSH levels, which differ between cell types. To achieve these aims, a multidisciplinary approach is strongly recommended, allowing a feedback loop between cell biologists and chemists in order to redesign aspects of the NP, with a view to tailoring the particles for specific cells and tissues.

Electronic Supplementary Material: Supplementary material (GSH intracellular levels in multiple cell types) is available in the online version of this article at http://dx.doi.org/ 10.1007/s12274-015-0828-5.

References

[1] Chiu, Y.-L.; Rana, T. M. siRNA function in RNAi: A chemical modification analysis. *RNA* **2003**, *9*, 1034–1048.

[2] Derfus, A. M.; Chen, A. A.; Min, D.-H.; Ruoslahti, E.; Bhatia, S. N. Targeted quantum dot conjugates for siRNA delivery. *Bioconjugate Chem.* **2007**, *18*, 1391–1396.

[3] Grigsby, C. L.; Leong, K. W. Balancing protection and release of DNA: Tools to address a bottleneck of non-viral gene delivery. *J. R. Soc. Interface* **2010**, *7*, S67–S82.

[4] Lévy, R.; Shaheen, U.; Cesbron, Y.; Sée, V. Gold nanoparticles delivery in mammalian live cells: A critical review. *Nano Rev.* **2010**, *1*, 4889.

[5] Karakoti, A. S.; Das, S.; Thevuthasan, S.; Seal, S. PEGylated inorganic nanoparticles. *Angew. Chem., Int. Ed.* **2011**, *50*, 1980–1994.

[6] Stefanick, J. F.; Ashley, J. D.; Kiziltepe, T.; Bilgicer, B. A systematic analysis of peptide linker length and liposomal polyethylene glycol coating on cellular uptake of peptide-targeted liposomes. *ACS Nano* **2013**, *7*, 2935–2947.

[7] Oishi, M.; Nakaogami, J.; Ishii, T.; Nagasaki, Y. Smart PEGylated gold nanoparticles for the cytoplasmic delivery of siRNA to induce enhanced gene silencing. *Chem. Lett.* **2001**, *35*, 1046–1047.

[8] Lushchak, V. I. Glutathione homeostasis and functions: Potential targets for medical interventions. *J. Amino Acids* **2012**, *2012*, 736837.

[9] Conde, J.; Tian, F. R.; Hernández, Y.; Bao, C. C.; Cui, D. X.; Janssen, K.-P.; Ibarra, M. R.; Baptista, P. V.; Stoeger, T.; de la Fuente, J. M. *In vivo* tumor targeting via nanoparticle-mediated therapeutic siRNA coupled to inflammatory response in lung cancer mouse models. *Biomaterials* **2013**, *34*, 7744–7753.

[10] Cebrián, V.; Martín-Saavedra, F.; Yagüe, C.; Arruebo, M.; Santamaría, J.; Vilaboa, N. Size-dependent transfection efficiency of PEI-coated gold nanoparticles. *Acta Biomater.* **2011**, *7*, 3645–3655.

[11] Dreaden, E. C.; Mackey, M. A.; Huang, X. H.; Kang, B.; El-Sayed, M. A. Beating cancer in multiple ways using nanogold. *Chem. Soc. Rev.* **2011**, *40*, 3391–3404.

[12] Conde, J.; Ambrosone, A.; Sanz, V.; Hernandez, Y.; Marchesano, V.; Tian, F. R.; Child, H.; Berry, C. C.; Ibarra, M. R.; Baptista, P. V. et al. Design of multifunctional gold nanoparticles for *in vitro* and *in vivo* gene silencing. *ACS Nano* **2012**, *6*, 8316–8324.

[13] Frens, G. Controlled nucleation for regulation of particle-size in monodisperse gold suspensions. *Nat. Phys. Sci.* **1973**, *241*, 20–22.

[14] Turkevich, J.; Stevenson, P. C.; Hillier, J. A study of the nucleation and growth processes in the synthesis of colloidal gold. *Discuss. Faraday Soc.* **1951**, 55–75.

[15] Lee, P. C.; Meisel, D. Adsorption and surface-enhanced Raman of dyes on silver and gold sols. *J. Phys. Chem.* **1982**, *86*, 3391–3395.

[16] McBeath, R.; Pirone, D. M.; Nelson, C. M.; Bhadriraju, K.; Chen, C. S. Cell shape, cytoskeletal tension, and RhoA regulate stem cell lineage commitment. *Dev. Cell* **2004**, *6*, 483–495.

[17] Conde, J.; Oliva, N.; Artzi, N. Implantable hydrogel embedded dark-gold nanoswitch as a theranostic probe to sense and overcome cancer multidrug resistance. *Proc. Natl. Acad. Sci. USA* **2015**, *112*, E1278–E1287.

[18] Ackerson, C. J.; Sykes, M. T.; Kornberg, R. D. Defined DNA/nanoparticle conjugates. *Proc. Natl. Acad. Sci. USA* **2005**, *102*, 13383–13385.

[19] Kumar, D.; Meenan, B. J.; Dixon, D. Glutathione-mediated release of Bodipy® from PEG cofunctionalized gold nanoparticles. *Int. J. Nanomedicine* **2012**, *7*, 4007–4022.

[20] Chompoosor, A.; Han, G.; Rotello, V. M. Charge dependence of ligand release and monolayer stability of gold nanoparticles by biogenic thiols. *Bioconjugate Chem.* **2008**, *19*, 1342–1345.

[21] Hong, R.; Han, G.; Fernández, J. M.; Kim, B.-J.; Forbes, N. S.; Rotello, V. M. Glutathione-mediated delivery and release using monolayer protected nanoparticle carriers. *J. Am. Chem. Soc.* **2006**, *128*, 1078–1079.

[22] Han, G.; Chari, N. S.; Verma, A.; Hong, R.; Marin, C. T.; Rotello, V. M. Controlled recovery of the transcription of nanoparticle-bound DNA by intracellular concentrations of glutathione. *Bioconjugate Chem.* **2005**, *16*, 1356–1359.

[23] Zhu, Z.-J.; Yeh, Y.-C.; Tang, R.; Yan, B.; Tamayo, J.; Vachet, R. W.; Rotello, V. M. Stability of quantum dots in live cells. *Nat. Chem.* **2011**, *3*, 963–968.

[24] Li, D.; Li, G. P.; Guo, W. W.; Li, P. C.; Wang, E. K.; Wang, J. Glutathione-mediated release of functional plasmid DNA from positively charged quantum dots. *Biomaterials* **2008**, *29*, 2776–2782.

[25] Meister, A.; Anderson, M. E. Glutathione. *Annu. Rev. Biochem.* **1983**, *52*, 711–760.

[26] Wu, G. Y.; Fan, Y.-Z.; Yang, S.; Lupton, J. R.; Turner, N. D. Glutathione metabolism and its implications for health. *J. Nutr.* **2004**, *134*, 489–492.

[27] Lei, X. G. *In vivo* antioxidant role of glutathione peroxidase: Evidence from knockout mice. *Methods Enzymol.* **2002**, *347*, 213–225.

[28] Fang, Y.-Z.; Yang, S.; Wu, G. Y. Free radicals, antioxidants, and nutrition. *Nutrition* **2002**, *18*, 872–879.

[29] Meister, A. Glutathione metabolism and its selective modification. *J. Biol. Chem.* **1988**, *263*, 17205–17208.

[30] Kah, J. C. Y.; Wong, K. Y.; Neoh, K. G.; Song, J. H.; Fu, J. W. P.; Mhaisalkar, S.; Olivo, M.; Richard, C. J. Critical parameters in the pegylation of gold nanoshells for biomedical applications: An *in vitro* macrophage study. *J. Drug Target.* **2009**, *17*, 181–193.

[31] Rana, T. M. Illuminating the silence: Understanding the structure and function of small RNAs. *Nat. Rev. Mol. Cell Biol.* **2007**, *8*, 23–36.

[32] Li, Z. H.; Rana, T. M. Molecular mechanisms of RNA-triggered gene silencing machineries. *Acc. Chem. Res.* **2012**, *45*, 1122–1131.

[33] Unsworth, L. D.; Sheardown, H.; Brash, J. L. Protein resistance of surfaces prepared by sorption of end-thiolated poly(ethylene glycol) to gold: Effect of surface chain density. *Langmuir* **2005**, *21*, 1036–1041.

[34] Knop, K.; Hoogenboom, R.; Fischer, D.; Schubert, U. S. Poly(ethylene glycol) in drug delivery: Pros and cons as well as potential alternatives. *Angew. Chem., Int. Ed.* **2010**, *49*, 6288–6308.

[35] Hinterwirth, H.; Kappel, S.; Waitz, T.; Prohaska, T.; Lindner, W.; Lämmerhofer, M. Quantifying thiol ligand density of self-assembled monolayers on gold nanoparticles by inductively coupled plasma-mass spectrometry. *ACS Nano* **2013**, *7*, 1129–1136.

[36] Häkkinen, H. The gold-sulfur interface at the nanoscale. *Nat. Chem.* **2012**, *4*, 443–455.